Chemistry Today

2026, Vol. 02 Issue 01
1-10

Research Article

Coprecipitation-Based Extraction of Nano-Hematite With The Effect of Dissolving Acid Strength

Muhammad Hanif Amrullah[1], Muhammad Rafli Akbar[2], Nurul Rosadinah[3], Yeni Ria Wulandari[4], Sukmaji Indro Cahyono[5], Amru Daulay[6], Singgih Prabowo[7], Sudibyo[8*]

[1,6,7,8]*Research Center for Mineral Technology, National Research and Innovation Agency (BRIN-Indonesia), Tanjung Bintang, Indonesia*
[2,3]*Department of Chemistry, Faculty of Mathematics and Natural Sciences, Lampung University, Bandar Lampung, Indonesia*
[4]*Department of Industrial Chemical Engineering Technology, Lampung State Polytechnic, Bandar Lampung, Indonesia*
[5]*Department of Mechanical Engineering, Faculty of Engineering, Sebelas Maret University, Surakarta, Indonesia*

ARTICLE INFORMATION

Received: Juny 29, 2026
Revised: September 9, 2026
Accepted: September 9, 2026
Available online: October 21, 2026

CORRESPONDENCE

E-mail: sudi014@brin.go.id

DOI
https://doi.org/10.68712/4bj7m849

A B S T R A C T

The coprecipitation-based extraction of hematite nanoparticles (nano-hematite, α-Fe_2O_3) from iron sand ore sampled at Tembakak Beach was studied as a function of acid concentration. The iron sand was dissolved in hydrochloric acid (HCl), then precipitated with ammonium hydroxide and calcined to produce nano-hematite. The as-extracted nano-hematite was characterized using elemental, crystal, and morphological analyses, employing XRF, XRD, and SEM, respectively. XRF data indicate that increasing the acid concentration significantly affects the yield of nano-hematite, with the highest product mass yield of 22.7% obtained using concentrated HCl (12 M). XRD analysis confirms the formation of the α-Fe_2O_3 crystalline phase, with a primary peak at 2θ = 33.16° and an average crystallite size of approximately 55.6 nm, as calculated using the Scherrer equation. Morphological characterization of extracted nano-hematite by SEM shows that it is in the form of nano-plates and rods that clump together. The results convincingly demonstrate that the HCl concentration during the dissolution stage strongly influences the yield of extracted nano-hematite.

Keywords: *Coprecipitation; Hydrochloric acid; Iron sand; Nano-hematite; Nanoparticle*

1. Introduction

Hematite is one of the most thermodynamically stable iron oxide phases, with a rhombohedral crystal structure and weak semiconductor & magnetic properties. This mineral has been extensively studied, perhaps owing to its wide range of potential applications, including catalysis, sensors/biosensors, environmental remediation, energy storage & conversion, and clinical applications. Nanoscale hematite (nano-hematite, α-Fe_2O_3) exhibits a significant increase in specific surface area, thereby enhancing surface activity relative to its bulk counterparts (Basavegowda, Mishra, & Lee, 2017; Tahir, Fakhar-e-Alam, Atif, Mustafa, & Ali, 2023; Xue & Wang, 2020). Obviously, this has prompted particular interest in developing strategies for synthesizing this nanomaterial.

To date, various synthesis methods have been developed to produce nano-hematite, which include sol-gel (Bagheri, KG, & Hamid, 2013), hydrothermal (Khalil, Yu, Liu, & Lee, 2014), microemulsion (Han, Liu, & Wei, 2011), and chemical precipitation (Supattarasakda, Petcharoen, Permpool, Sirivat, & Lerdwijitjarud, 2013). Among the methods, coprecipitation is a straightforward, cost-efficient approach that can produce nanoparticles with good crystallinity by adjusting specific reaction parameters (Dissanayake et al., 2019; Farahmandjou & Soflaee, 2015; Shivani, Bhat, Sajankila, & Ag, 2025). This process generally involves

This is an open-access article distributed under the terms of the Creative Commons Attribution-NonCommercial-ShareAlike 4.0 International.

dissolving iron precursors, precipitating ferric (Fe^{3+}) ions with a base, and calcining to obtain the α-Fe_2O_3 phase (Farahmandjou & Soflaee, 2015; Tahir et al., 2023).

Synthesis parameters, such as pH, calcination temperature, precursor concentration, and annealing conditions, were shown to significantly affect the crystallite size, phase purity, and morphology of the resulting hematite nanoparticles (Dissanayake et al., 2019; Farahmandjou & Soflaee, 2015; Shivani et al., 2025). Further, the use of stabilizing/capping agents and environmentally friendly synthesis methods has also been found to enhance control over particle size distribution and stability (Ahmmad et al., 2013; Basavegowda et al., 2017; Hutapea et al., 2026; Park, Jung, Lee, & Cho, 2016). However, most studies only focus on optimizing temperature, pH, or the use of additives (Aliyu, Yabagi, Ladan, & Erena, 2025; Dissanayake et al., 2019; Farahmandjou & Soflaee, 2015; Sitorus, Manulang, Sasri, & Panjaitan, 2025; Yudhistira et al., 2026).

In the present study, particular attention was given to the influence of HCl concentration on the coprecipitation behavior under the investigated system and operating conditions. Therefore, the contribution of this work was focused on clarifying the effect of HCl concentration within this specific experimental framework rather than claiming that this parameter has not been previously investigated. Additionally, the characteristics of the extracted nano-hematite, including α-Fe_2O_3 phase purity, crystallite size, and morphology, were studied. These characteristics were thoroughly examined using XRF, XRD, and SEM-EDS. The approach provided a deeper understanding of the role of acid concentration in nano-hematite synthesis and laid the foundation for developing more efficient, controlled synthesis methods.

2. Methods

2.1 Materials and Instruments

Iron sand ore was obtained from Tembakak Beach, Pesisir Barat Regency, Lampung Province, Indonesia. Ammonium hydroxide (NH_4OH) and hydrochloric acid (HCl) were purchased from Sigma-Aldrich. All aqueous solutions were prepared using ultrapure water with a resistivity of 18.2 MΩ·cm using Millipore Milli-Q water purification equipment.

A set of glassware, a 325-mesh sieve, a magnetic stirrer, an oven, a muffle furnace, a planetary ball mill, and other process instruments were used in this research. Elemental, chemical, and structural analyses were performed using a Panalytical Epsilon 3 XLE X-ray fluorescence (XRF) spectrometer. Crystal phase and lattice parameters were examined employing X-ray diffraction (XRD), Panalytical X'Pert^3 Powder. The crystallite size was calculated from XRD data using the Scherrer equation, which relates diffraction peak broadening to crystallite size on the nanometre scale. The nano-hematite's surface morphology, particle distribution, and elemental mapping were studied using scanning electron microscopy-energy dispersive spectroscopy (SEM-EDS), Thermo Scientific Quattro S. All experiments were done at the Research Center for Mineral Technology, National Research and Innovation Agency (BRIN), Indonesia.

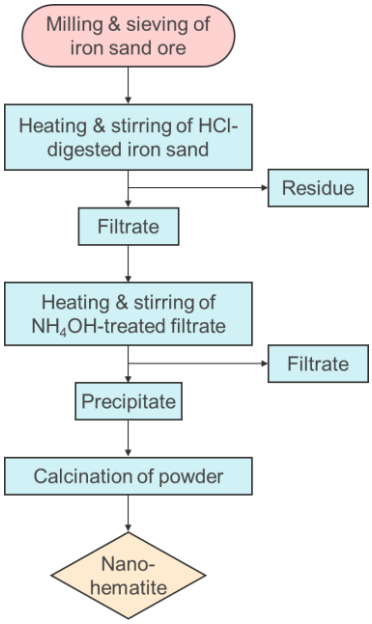


Figure 1. Schematic diagram illustrating the synthesis of nano-hematite from iron sand ore.

 https://doi.org/10.68712/4bj7m849

2.2 Procedures

Iron sand samples were naturally dried, then magnetically separated with a magnetic rod to remove non-magnetic minerals. The separated iron sand was ground in a planetary ball mill at 300 rpm for 30 min, then sieved through a 325-mesh sieve. Nano-hematite extraction was performed via coprecipitation. A total of 50 g of iron sand was dissolved separately in 150 mL of 8, 10, and 12 M HCl, and the acid-treated iron sand was heated at 110 ºC for 30 min under stirring. The resulting solution was filtered to separate the solid residue. The filtrate was then gradually added to a 25% NH_4OH solution, heated to 80 °C, and stirred continuously until the pH reached 6, as indicated by the formation of a reddish-brown precipitate. The precipitate was washed repeatedly with distilled water until a clear filtrate was obtained, then dried at 150 °C for 3 h. The dried powder was then calcined at 700 ºC for 2 h using a muffle furnace to convert the phase to the nanoscale. All experiments and analyses were carried out in triplicate. Figure 1 shows a flowsheet of the stepwise coprecipitation-based nano-hematite extraction process.

3. Results and Discussion

3.1 Coprecipitation-based extraction of nano-hematite

Nano-hematite extraction by coprecipitation was studied using 8, 10, and 12 M HCl solutions. Table 1 shows how varying the concentration of the HCl solution affects the mass of the product obtained and the corresponding percentage product mass yield, while keeping the initial mass of the starting material constant. The increasing HCl concentration from 8 to 12 M consistently increases both the mass of coprecipitated product and the product mass yield when processing 50 g of iron sand. At 8 M HCl, 9.47 g of product was obtained (18.9%), which increased to 10.19 g (20.4%) at 10 M and reached a maximum of 11.36 g (22.7%) at 12 M. The One-Way ANOVA showed that the % product differed significantly across acid concentrations (Table 2). One-way ANOVA demonstrated a statistically significant effect of treatment/group on the measured response, $F(2,6) = 10.23$, $p = 0.0117$. The mean response decreased from 22.72 ± 1.14 for Group 1 to 20.38 ± 1.01 for Group 2 and 18.94 ± 0.94 for Group 3. The model explained approximately 77.3% of the total variation ($R^2 = 0.773$). Therefore, the null hypothesis of equal means was rejected, indicating that at least one treatment level differs significantly from the others. The monotonic trend indicates that stronger acid promotes more effective dissolution of iron sand ore during the digestion stage, producing higher concentrations of soluble Fe ions that later form solid precipitates during coprecipitation by NH_4OH. Otherwise, lower HCl concentrations leave more minerals undissolved and reduce the amount of recovered nano-hematite product. After calcination, a brick-red powder, characteristic of Fe_2O_3, was obtained, as shown in Figure 2. Acid concentration is an important parameter for optimizing nano-hematite extraction via coprecipitation.

Table 1. Effect of HCl concentration on product mass yield (constant starting mass = 50 g).

Concentration of HCL solution (M)	Mass of starting material (g)	Mass of obtained product (g)	Product mass yield (%)
12	50	11.36 ± 0.6	22.72 ± 1.14
10	50	10.19 ± 0.51	20.38 ± 1
8	50	9.47 ± 0.47	18.94 ± 0.94

Table 2. Statistical comparison of product mass yield at different acid concentrations using One-Way ANOVA.

a) Descriptive statistics

[HCl]/M	%Mean	SD	SE of Mean
12	22.72	1.14	0.66
10	20.38	1.01	0.58
8	18.94	0.94	0.54

b) One-way ANOVA

DF	Sum of Squares	Mean square	F Value	Prob>F
2	21.84	10.92	10.23	0.01165
6	6.4	1.07		
8	28.24			

c) Fit Statistics

R-Square	Coeff Var	Root MSE	Data Mean
0.773	0.05	1.03	20.68



Figure 2. Nano-hematite extracted from iron sand by coprecipitation with various concentrations of HCl: a) 8 M, b) 10 M, and c) 12 M.

The formation of nano-hematite from iron sand using HCl and NH_4OH is shown in the following reactions.

$Fe_2O_3 + 6HCl \rightarrow 2FeCl_3 + 3H_2O$ .....(1)

$FeCl_3 + 3NH_4OH \rightarrow Fe(OH)_3 + 3NH_4Cl$ .....(2)

$Fe(OH)_3 \rightarrow FeOOH + H_2O$ .....(3)

$2FeOOH \rightarrow Fe_2O_3 + H_2O$ .....(4)

3.2 XRF analysis of extracted nano-hematite

To determine the elemental composition of the extracted nano-hematite relative to the raw material (iron sand ore), XRF analysis was conducted on both samples. The results obtained from the XRF analysis are presented in detail in Table 3, which collectively illustrate the elemental composition and quantitative distribution of the samples. The initial iron sand raw material primarily consists of Fe at 58.3%, followed by concentrations of Si at 18.5%, Ti at 8.4%, Al at 6.8%, and K at 1.6%, with the remaining elements present in trace amounts below 0.5%. These results indicate that iron sand has a high iron content and is dominated by magnetic minerals. Among oxide compounds, the most abundant is Fe_2O_3 with a content of approximately 47.4%, followed by SiO_2 (27.6%), TiO_2 (9.3%), Al_2O_3 (9.1%), CaO (3.4%), K_2O (1.3%), and others (< 1%). The dominance of Fe_2O_3 indicates that this iron sand ore has high potential as a hematite source.

Table 3. Elemental and oxide composition of iron sand ore, showing initial concentrations and the variation in residual concentrations after acid digestion, highlighting the effect of acid strength on impurity removal and iron enrichment.

Raw material				Product		
Element	Concentration (%)	Compound	Concentration (%)	Concentration after HCl dissolution (%)		
				8 M	10 M	12 M
Fe	58.3	Fe_2O_3	47.4	87.8	90.5	91.1
Si	18.5	SiO_2	27.6	-	-	-
Ti	8.4	TiO_2	9.3	10.4	7.3	7.2
Al	6.8	Al_2O_3	9.1	-	-	-
Ca	0.2	CaO	3.4	0.2	0.2	0.1
K	1.6	K_2O	1.3	-	-	-
P	0.3	P_2O_5	0.4	-	-	-
V	0.6	V_2O_5	0.4	0.8	0.7	0.8
Mn	0.2	MnO	0.3	0.1	0.4	0.07
Sn	0.1	SnO_2	0.1	0.1	0.1	-
Cr	0.1	Cr_2O_3	0.08	0.1	0.1	0.2
Zn	0.08	ZnO	0.07	0.07	0.1	0.08
Sb	0.1	Sb_2O_3	0.06	0.08	0.07	0.07

 https://doi.org/10.68712/4bj7m849

Raw material				Product		
Element	Concentration (%)	Compound	Concentration (%)	Concentration after HCl dissolution (%)		
				8 M	10 M	12 M
Ni	0.07	NiO	0.03	0.06	0.04	0.04
Eu	0.3	Eu_2O_3	0.2	-	0.2	0.1
Zr	0.02	ZrO_2	0.05	0.02	0.01	0.01
Sr	0.003	SrO	0.04	-	0.002	-
Pb	0.06	PbO	0.03	0.05	-	-
Rb	0.04	Rb_2O	0.02	0.03	0.02	0.03
Te	0.009	TeO_2	0.01	0.008	0.007	0.009
Nb	0.009	Nb_2O_5	0.006	-	-	-
Bi	0.04	Bi_2O_3	0.005	0.03	0.03	0.03
Yb	0.05	Yb_2O_3	-	0.04	0.05	0.04
Ir	0.05	IrO_2	-	0.04	-	-
Cu	0.03	CuO	-	0.02	-	-
Sc	0.01	Sc_2O_3	-	0.02	-	0.02
Os	0.01	OsO_4	-	0.01	-	-
Hf	0.05	HfO_2	-	-	0.04	-
Ga	0.01	Ga_2O_3	-	-	0.01	0.02
Se	0.003	SeO_2	-	-	0.003	-

(-) means “not detected.”

XRF analysis revealed that the nano-hematite content increased substantially after extraction, particularly at HCl concentrations of 8, 10, and 12 M, compared with the raw material. In the initial material of iron sand ore, the Fe_2O_3 content was 47.4%; after extraction, it increased to 87.8% (8 M HCl), 90.5% (10 M HCl), and reached a maximum of 91.1% at 12 M HCl. This trend confirms that an increase in acid concentration plays an important role in enriching iron materials by first increasing the solubility of iron oxide and the concentration of Fe^{3+} ions in solution, and then promoting precipitation.

3.3 XRD analysis of extracted nano-hematite

XRD analysis was carried out to determine the phase, crystal structure, lattice parameters, and crystal size of extracted iron-sand-derived nano-hematite, and to confirm the 2θ peaks. The results of XRD characterization, in the form of a diffractogram showing 2θ diffraction angles and intensities, were analyzed using HighScore Plus (HSP) software. Each material produces a distinctive diffraction pattern. XRD measurements were done at λ = 1.54 Å in the 2θ diffraction angle range (10°-100°). Afterward, the 2θ diffraction angle data were compared with the literature, and the diffractogram data were used to identify the crystal structure and phase using the Crystallography Open Database (COD).

The XRD diffractogram shows the main diffraction peaks at 2θ angles of 24.15°, 33.16°, 35.63°, 40.88°, 49.47°, 54.09°, 57.64°, 62.43°, and 64.00° (Figure 3a). The highest peak is observed at an angle of 2θ = 33.16°, which is characteristic of the (104) crystal plane of the nano-hematite phase.

The Fe_2O_3 crystallite size was determined using the Scherrer equation based on the highest diffraction peak at an angle of 2θ = 33.16° with a Full Width at Half Maximum (FWHM) value of 0.15°. Based on Crystallography Open Database (COD) data with reference code 96-900-4143 at the 2θ peak of 72.03°, the phase formed is hematite (α-Fe_2O_3), and the crystal structure obtained is trigonal (hexagonal axes) with α = β = 90° and γ = 120°, and the lattice parameters obtained are *a* = 5.03 Å and c = 13.75 Å. The crystal structure of nano-hematite can be shown in Figure 3b. Using a crystal shape constant (K) of 0.9 and a Cu-Kα X-ray wavelength of 1.5406 Å, the crystallite size was 55.6 nm. This value indicates that the produced Fe_2O_3 is nanometre-scale and classified as nanoparticles (Cullity & Stock, 2014; Patterson, 1939).

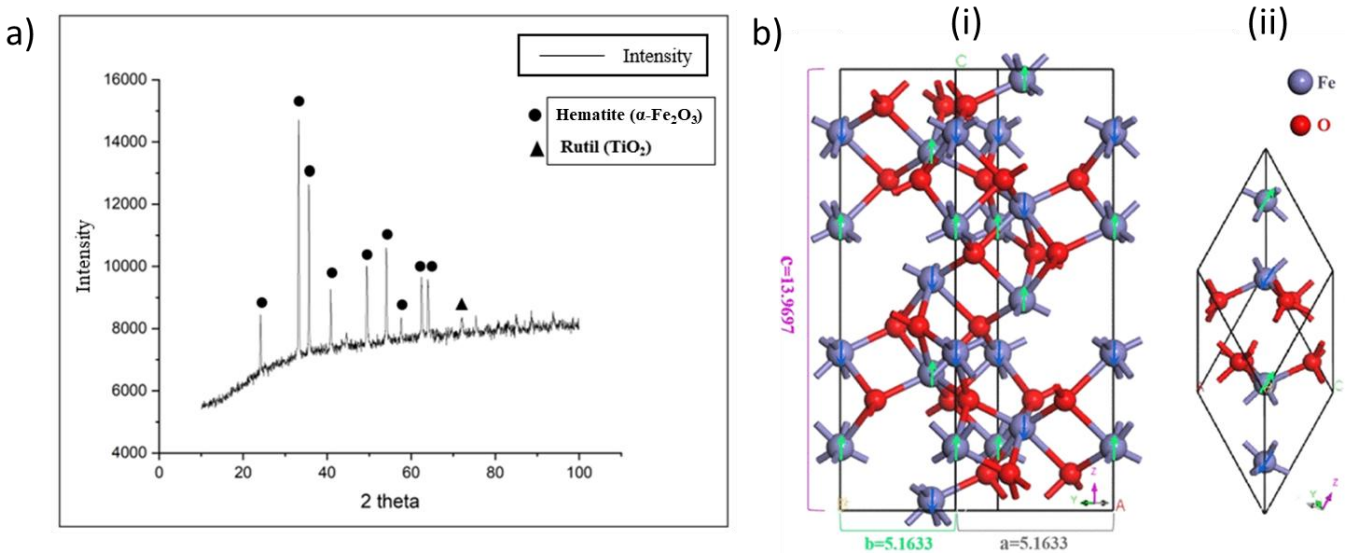


Figure 3. a) XRD diffractogram from the extracted product. b) Hematite crystal structures for (i) optimized structure of the hematite bulk cell and (ii) rhombohedral unit cell of the optimized bulk cell, from (Zhang, Sun, Xie, He, & Zhang, 2023). Copyright © 2023 The Authors. Published by the American Chemical Society.

The diffraction pattern is consistent with the Joint Committee on Powder Diffraction Standards (JCPDS) standard card (No. 33-0664) for hematite, which has a hexagonal crystal structure. This confirms that coprecipitation, followed by calcination at 700 °C, successfully promoted phase transformation and crystallization. In addition, a minor peak related to the rutile phase (TiO_2) was detected, indicating the presence of a small amount of TiO_2 impurities, in line with the results of the previous XRF analysis. The XRD data obtained are in accordance with the literature. As in a study reported by Zanur et. al. (Zanur, Putra, & Astuti, 2017), the XRD results showed the highest peak at an angle of 2θ = 33.11° and a FWHM value of 0.13. The phase formed is hematite (α-Fe_2O_3), which has a rhombohedral-hexagonal crystal structure. The same results were obtained in Fahlepy et al.'s investigation: the phase formed was hematite (α-Fe_2O_3), with a 2θ angle of 33.20°, and the crystal structure was hexagonal, space group R-3c (Fahlepy, Wahyuni, Andhika, Vistarani, & Subaer, 2019).

The relatively small crystallite size indicates that coprecipitation can effectively control crystal growth, especially when pH is controlled and calcination is carried out under controlled conditions. These results are consistent with previous reports indicating that coprecipitation is an efficient method for producing hematite nanoparticles with crystallite sizes below 100 nm (Hui & Salimi, 2020; Husain et al., 2024). Confirmation of the XRF analysis is provided by the successful synthesis of nano-hematite, which also indicates that the extraction process with 12 M HCl is most effective for producing high-yield α-Fe_2O_3 with a nanocrystalline structure.

The XRD data were used to calculate crystallite size using the Scherrer equation, thereby determining the crystallite size for each extracted product. The Scherrer equation can be expressed in the following equation:

$$D = \frac{K\lambda}{\beta\cos\theta}$$

Where D is the average crystal size, λ is the wavelength of X-ray radiation, K is the Scherrer constant, β is the magnitude of the broadening at half the height of the maximum diffraction peak or based on full width at half maximum, and θ is the diffraction angle.

In calculating the crystallite size, the highest-intensity peak (2θ = 33.16°) is used, with an FWHM of 0.15°. This is because the hematite phase forms the highest peak and is more dominant than the other diffraction peaks. The nano-hematite crystal size was calculated using the Scherrer equation, as below, yielding a crystallite size of 55.6 nm.

K = 0.9 (constant)
λ = 1.54 Å
β = $0.15^o \rightarrow 0.15\pi/180 = 0.0026$ rad

$$D = \frac{K\lambda}{\beta\cos\theta}$$

https://doi.org/10.68712/4bj7m849

$2\theta = 33.16^{o}$
$\theta = 16.58°$

$$D = \frac{0.9 \times 1.54}{0.0026 \times \cos(16.58)}$$
$$D = \frac{1.39}{0.0026 \times 0.96}$$
$$D = \frac{1.39}{0.0025}$$
$$D = 556 \text{ Å or } 55.6 \text{ nm}$$

Based on the analyses, TiO_2 was detected only in a small amount, indicating that hematite remains the dominant phase in the synthesized product. At this concentration, the TiO_2 impurity is unlikely to significantly affect applications in which nano-hematite is used as an adsorbent, catalyst support, or pigment precursor, since a minor titanium oxide content is unlikely to substantially alter the material's overall physicochemical properties. In some cases, trace TiO_2 may even contribute positively to photocatalytic or surface-related properties. However, we acknowledge that for high-purity applications, such as electronic materials, magnetic devices, or specialized biomedical uses, further purification may be required. Potential removal strategies include selective acid leaching, alkali treatment, or additional purification steps during precursor separation to reduce the amount of titanium-containing phases.

3.4 Morphology analysis of nano-hematite

SEM analysis for extracted nano-hematite was carried out at magnifications of 1,000×, 5,000×, and 10,000×. At a 1,000× magnification (Figure 4a), the α-Fe_2O_3 particles are seen to form micrometer-sized agglomerates, and their distribution is relatively inhomogeneous. This agglomeration is common among metal oxide nanoparticles due to intermolecular forces and high surface energy during drying and calcination. At a higher magnification of 5,000× (Figure 4b), the particle structure becomes clearer, with a dominant morphology of plate-like and rod-like particles stacked on top of each other. This morphology is characteristic of hematite, which forms via anisotropic crystal growth during calcination. The presence of these elongated structures indicates a controlled nucleation and crystal growth process during coprecipitation. At 10,000× magnification (Figure 4c), the primary particles are homogeneous, nanometer-sized, and form secondary agglomerates. Even though the particles undergo agglomeration, the constituent crystallites remain nanoscale. SEM results reinforce the XRD characterization results and confirm the successful synthesis of nano-hematite using the coprecipitation method.

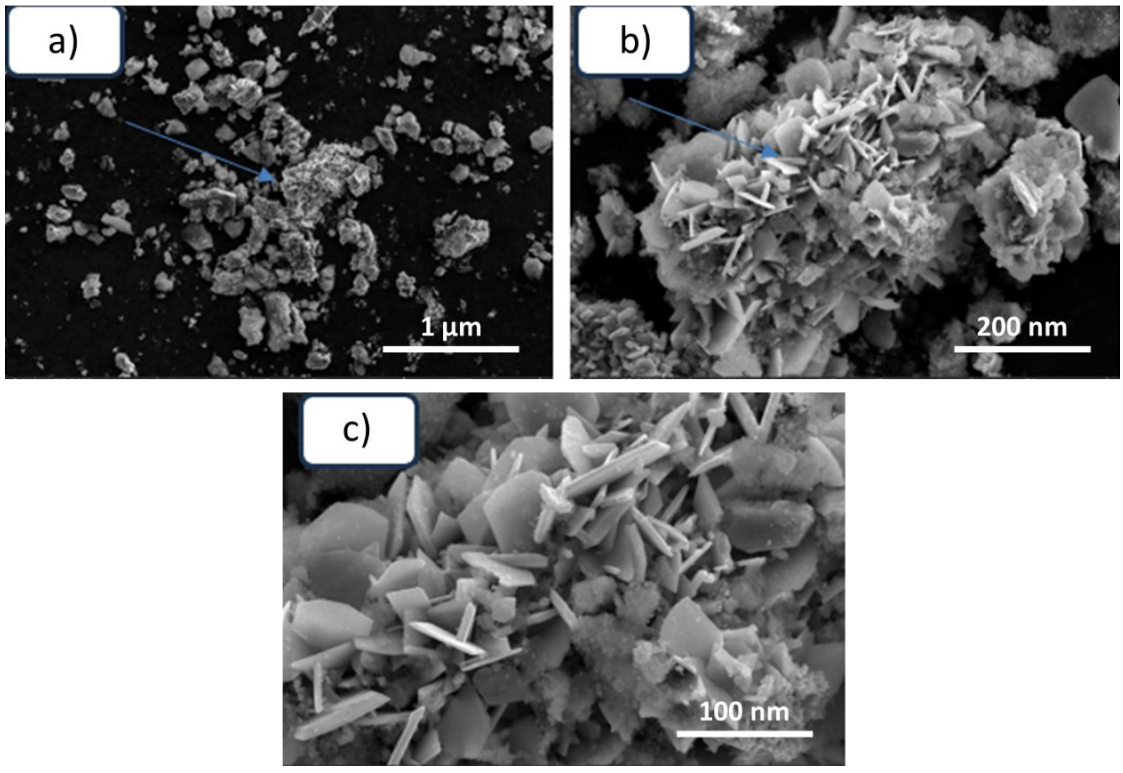


Figure 4. SEM images of extracted α-Fe_2O_3 at magnifications of a) 1,000×, b) 5,000×, and c) 10,000×

Further, the elemental mapping images of nano-hematite particles clearly show the presence of Fe, O, C, Al, Ti, and V (Figure 5(a-g)). The inset of Figure 5 shows an SEM image of nano-hematite at a magnification of 5,000×. Table 3 presents the elemental composition of extracted α-Fe_2O_3, including atomic number, measured mass percentage, reference (normal) mass percentage, atomic percentage, and associated uncertainties expressed as absolute and relative errors (1-sigma). Iron is the predominant element, comprising 68.3% by mass compared to a normal value of 69.8%. In this regard, normal mass represents the relative composition, assuming the detected elements account for 100% of the analyzed composition. It also has the highest atomic fraction at 40.1%. The absolute error for iron is 1.7%, and the relative error is 2.5%. Oxygen is the second most abundant element, contributing 16.1% by mass and 32.9% by atomic percentage. Its relative error is 4.8%, reflecting moderate uncertainty. Carbon makes up 8% by mass but 21.8% by atoms, illustrating how lighter elements contribute more significantly to atomic percentage. Carbon shows the highest relative error (5.7%). Minor constituents include Al, Ti, and V, each below 3% by mass. Among these, Ti has the lowest relative error (3%), while vanadium exhibits one of the highest (5.7%), despite its small concentration. Overall, the measured mass percentages closely match the normal values, suggesting reliable analytical performance. Although a low percentage of interfering elements was found in the extracted α-Fe_2O_3, this raises concerns about the specific precipitation of iron species.

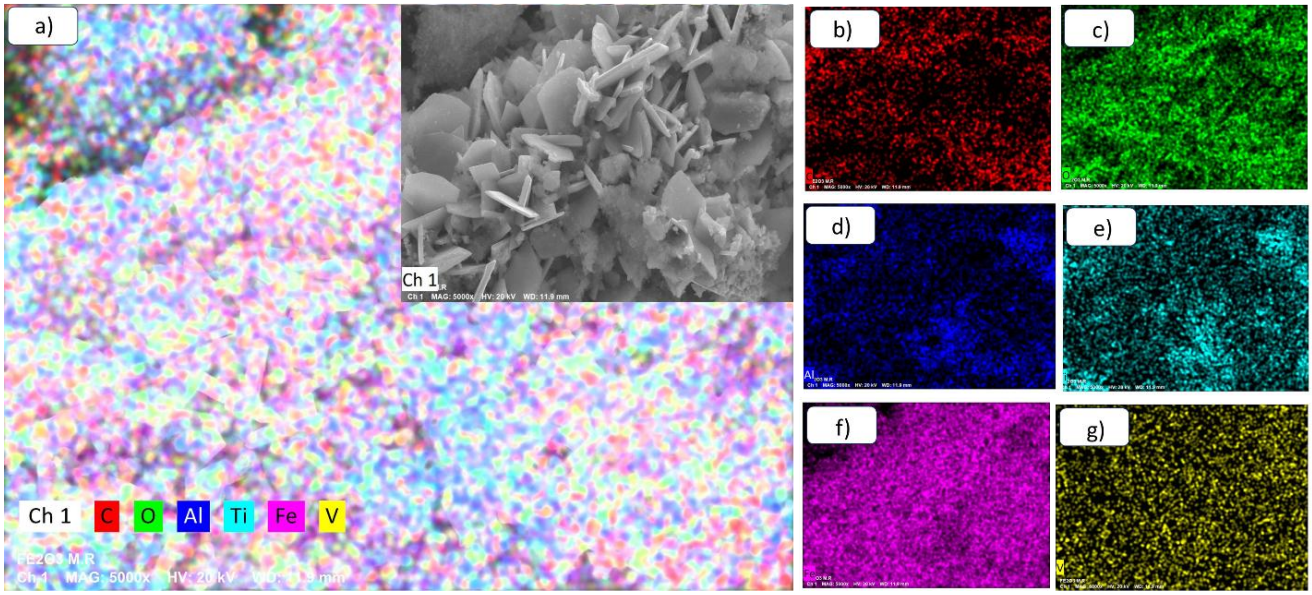


Figure 5. a) Elemental mapping of extracted nano-hematite, inset of a) SEM image with magnification of 5,000×. Element distribution of b) C, c) O, d) Al, e) Ti, f) Fe, and g) V. All analyses were performed for a 12 M HCl solution.

Table 4. Elemental composition of extracted α-Fe_2O_3 showing atomic number, measured & reference mass percentages, atomic percentage, and associated absolute & relative errors.

Element	Atomic number	Mass (%)	Normal mass (%)	Atom (%)	Abs Error (%) (1-sigma/1σ)	Rel. Error (%) (1-sigma/1σ)
Fe	26	68.3	69.8	40.1	1.7	2.5
O	8	16.1	16.4	32.9	0.8	4.8
C	6	8	8.2	21.8	0.5	5.7
Al	13	2.8	2.8	3.4	0.1	5.2
Ti	22	2.2	2.2	1.5	0.07	3
V	23	0.6	0.6	0.4	0.03	5.7

1-sigma (1σ) refers to the standard deviation of a measurement expressed as a fraction or percentage of the measured value, representing a 68.3% confidence interval.

The detected carbon signal in Table 4 likely originated from two sources: (i) carbon tape/coating used during SEM-EDS sample preparation and (ii) residual carbonate impurities naturally present in the raw iron sand, such as $CaCO_3$. SEM-EDS can detect C content, whereas XRF cannot.

 https://doi.org/10.68712/4bj7m849

4. Conclusion

The coprecipitation method is effective for extracting nano-hematite from natural iron sand ore by controlling the HCl concentration, a key parameter. Increasing the HCl concentration from 8 to 12 M consistently increased the yield of nano-hematite, with the highest content of about 91.1% obtained at 12 M HCl, the best condition within the tested range. XRD characterization confirmed the formation of a hexagonal hematite phase with a crystallite size of approximately 55.6 nm, indicating nanoparticle-scale dimensions, and SEM results revealed a relatively homogeneous morphology. Adjusting the acid solvent concentration is key to producing well-formed hematite nanoparticles from iron sand, as these findings show. This provides a solid foundation for further development of natural-source-derived nanoparticle extraction for a wide range of applications. Future work should use an experimental design/design of experiments (DoE) to systematically optimize key parameters and identify the optimal conditions, rather than changing one factor at a time. Using screening followed by response-surface optimization with replicates and statistical analysis will improve reproducibility, reveal factor interactions, and deliver more reliable, high-performance results.

Acknowledgement

The authors thank the editor and referees for their comments and useful suggestions.

Funding

This work was funded in part by the Research Organization for Nanotechnology and Materials – National Research and Innovation Agency (BRIN) research grant 2026.

References

Ahmmad, B., Leonard, K., Shariful Islam, M., Kurawaki, J., Muruganandham, M., Ohkubo, T., & Kuroda, Y. (2013). Green synthesis of mesoporous hematite (α-Fe2O3) nanoparticles and their photocatalytic activity. *Advanced Powder Technology, 24*(1), 160-167. doi:10.1016/j.apt.2012.04.005

Aliyu, A., Yabagi, J. A., Ladan, M. B., & Erena, F. A. (2025). Solvent-dependent synthesis and optical characterization of iron oxide (Fe₂O₃) nanoparticles via coprecipitation method. *Science World Journal, 20*(3), 1065-1071. doi:10.4314/swj.v20i3.21

Bagheri, S., KG, C., & Hamid, S. B. A. (2013). Generation of hematite nanoparticles via Sol-Gel method. *Research Journal of Chemical Sciences, 3*(7), 62-68. Retrieved from https://www.researchgate.net/publication/272942069_Generation_of_Hematite_Nanoparticles_via_Sol-Gel_Method

Basavegowda, N., Mishra, K., & Lee, Y. R. (2017). Synthesis, characterization, and catalytic applications of hematite (α-Fe2O3) nanoparticles as reusable nanocatalyst. *Advances in Natural Sciences: Nanoscience and Nanotechnology, 8*(2). doi:10.1088/2043-6254/aa6885

Cullity, B. D., & Stock, S. R. (2014). *Elements of X-ray Diffraction*: Pearson Education.

Dissanayake, D. M. S. N., Mantilaka, M. M. M. G. P. G., Palihawadana, T. C., Chandrakumara, G. T. D., De Silva, R. T., Pitawala, H. M. T. G. A., . . . Amaratunga, G. A. J. (2019). Facile and low-cost synthesis of pure hematite (α-Fe2O3) nanoparticles from naturally occurring laterites and their superior adsorption capability towards acid-dyes. *RSC Advances, 9*(37), 21249-21257. doi:10.1039/c9ra03756j

Fahlepy, M. R., Wahyuni, Y., Andhika, M., Vistarani, A. T., & Subaer, S. (2019). Synthesis and Characterization of Nanoparticles Hematite (α-Fe₂O₃) Minerals from Natural Iron Sand Using Co-Precipitation Method and its Potential Applications as Extrinsic Semiconductor Materials Type-N. *Materials Science Forum, 967*, 259-266. doi:10.4028/www.scientific.net/MSF.967.259

Farahmandjou, M., & Soflaee, F. (2015). Synthesis and characterization of α-Fe2O3 nanoparticles by simple co-precipitation method. *Physical Chemistry Research, 3*, 193-198. doi:https://doi.org/10.22036/pcr.2015.9193

Han, L.-H., Liu, H., & Wei, Y. (2011). In situ synthesis of hematite nanoparticles using a low-temperature microemulsion method. *Powder Technology, 207*(1-3), 42-46. doi:10.1016/j.powtec.2010.10.008

Hui, B. H., & Salimi, M. N. (2020). Production of Iron Oxide Nanoparticles by Co-Precipitation method with Optimization Studies of Processing Temperature, pH and Stirring Rate. *IOP Conference Series: Materials Science and Engineering, 743*(1). doi:10.1088/1757-899x/743/1/012036

Husain, H., Adi, W. A., Subaer, S., Taryana, Y., Setiawan, A., Putri, S. E., . . . Wannapaiboon, S. (2024). Effect of calcination temperature on structure evolution of hematite nanoparticles. *Physica Scripta, 99*(6). doi:10.1088/1402-4896/ad48cd

Hutapea, T. P. H., Lembang, M. S., Huda, A., Asranudin, Dewi, D. P., Suprapto, . . . Norrrahim, M. N. F. (2026). Nypa fruticans-assisted green-synthesized gold nanoparticles for an enhanced electrochemical formaldehyde sensor based on fish albumin composite. *Global Journal of Environmental Science & Management, 12*(1), 95-110. doi:10.22034/gjesm.2026.01.06

Khalil, M., Yu, J., Liu, N., & Lee, R. L. (2014). Hydrothermal synthesis, characterization, and growth mechanism of hematite nanoparticles. *Journal of Nanoparticle Research, 16*(4). doi:10.1007/s11051-014-2362-x

Park, C., Jung, J., Lee, C. W., & Cho, J. (2016). Synthesis of Mesoporous α-Fe2O3 Nanoparticles by Non-ionic Soft Template and Their Applications to Heavy Oil Upgrading. *Scientific Reports, 6*(1). doi:10.1038/srep39136

Patterson, A. L. (1939). The Scherrer Formula for X-Ray Particle Size Determination. *Physical Review, 56*(10), 978-982. doi:10.1103/PhysRev.56.978

Shivani, Bhat, R. S., Sajankila, S. P., & Ag, B. (2025). Iron oxide (α-Fe2O3) nanoparticles: synthesis, characterization, and the degradation of methyl red. *Applied Physics A, 131*(8). doi:10.1007/s00339-025-08775-6

Sitorus, B., Manulang, Y. A. A., Sasri, R., & Panjaitan, S. D. (2025). Synthesis and Characterization of Hematite (α-Fe_2O_3) Nanomaterials from Red Mud Using EDTA as Capping Agent. *Jurnal Kimia Sains dan Aplikasi, 28*(8), 463-470. doi:10.14710/jksa.28.8.463-470

Supattarasakda, K., Petcharoen, K., Permpool, T., Sirivat, A., & Lerdwijitjarud, W. (2013). Control of hematite nanoparticle size and shape by the chemical precipitation method. *Powder Technology, 249*, 353-359. doi:10.1016/j.powtec.2013.08.042

Tahir, M., Fakhar-e-Alam, M., Atif, M., Mustafa, G., & Ali, Z. (2023). Investigation of optical, electrical and magnetic properties of hematite α-Fe2O3 nanoparticles via sol-gel and co-precipitation method. *Journal of King Saud University - Science, 35*(5). doi:10.1016/j.jksus.2023.102695

Xue, Y., & Wang, Y. (2020). A review of the α-Fe2O3 (hematite) nanotube structure: recent advances in synthesis, characterization, and applications. *Nanoscale, 12*(20), 10912-10932. doi:10.1039/d0nr02705g

Yudhistira, N., Padmasari, R., Puspitawati, I. N., Muljani, S., Sani, S., & Ramandani, A. A. (2026). Optimization of alpha-Fe2O3 Synthesis from Iron Sand via Extraction–Precipitation using Response Surface Methodology. *AJARCDE (Asian Journal of Applied Research for Community Development and Empowerment), 10*(1), 96-101. doi:10.29165/ajarcde.v10i1.889

Zanur, H., Putra, A., & Astuti, A. (2017). Sintesis Dan Karakterisasi Pigmen Hematit (Î±-Fe2O3) Dari Bijih Besi Di Jorong Kepalo Bukik Kabupaten Solok Selatan Menggunakan Metode Presipitasi. *Jurnal Fisika Unand, 6*(2), 149-155. doi:10.25077/jfu.6.2.149-155.2017

Zhang, H., Sun, W., Xie, X., He, J., & Zhang, C. (2023). Insights into the Fracture Nature of Hematite from First Principles DFT Calculations. *ACS Omega, 8*(9), 8248-8255. doi:10.1021/acsomega.2c06101